Supplementary Material

Application of static integrated skeletal reduction and tabulation of dynamic adaptive chemistry in the combustion simulation of ethylene-fueled scramjet combustor

Zhongwen Li [a,b], Jianwen Liu [c] and Jingbo Wang [*,a,b]

[a] School of Chemical Engineering, Sichuan University, Chengdu, 610065, P. R. China

[b] Engineering Research Center of Combustion and Cooling for Aerospace Power, Ministry of Education, Sichuan University, Chengdu, 610065, P. R. China

[c] Beijing Power Machinery Institute, Beijing, 100074, P. R. China

Corresponding author: wangjingbo@scu.edu.cn

Content

Mesh independent analysis

Mesh independent analysis is carried out based on non-reactive flow field of no-fuel injection to choose proper mesh resolution by employing three meshes respectively consisting of 3.26, 4.89, 7.33 million cells. Fig. S1 shows the influence of mesh resolution on pressure profile along the upper wall in the non-reactive flow. In order to show more intuitively the distribution characteristics of pressure and shock wave structure, their contours for the central cross-section of medium mesh are given in the upper and lower parts of the figure. As can be seen, all the three meshes offer the same trend of the pressure distribution with negligible difference and they are qualified for accurately capture the shock waves and their interactions in this combustor. The first pressure drop is in the unilaterally diverging combustion section I, and the second pressure drop is in the T1 cavity. The impact of the shear layer of the T1 cavity with the oblique shock wave generated at the trailing edge of the T1 cavity leads to a sharp rise in pressure, and the pressure rises again when the oblique shock wave is reflected to the upper wall. Considering the accuracy and computational cost, the medium mesh of 4.89 million cells is adopted for subsequent combustion simulations.
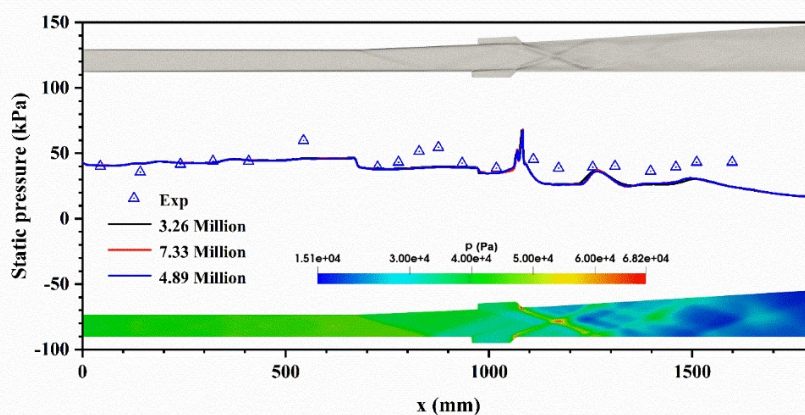

Fig. S1. The influence of mesh resolution on pressure profile along the upper wall in cold flow field.

Comparisons on kinetic performance for related ethylene mechanisms

Considering the related skeletal mechanisms applicable to ethylene combustion in the literature review in the introduction section (as summarized in Table 1), the work in this part systematically carries out comparisons of the kinetic performances of the skeletal mechanisms of 24S-86R [11], 35S-228R [49], 38S-230R [63], and 70S-451R [44] with the skeletal mechanism 26S-117R obtained by the present integrated reduction methods. These mechanisms are selected according to the applicability of their reduction conditions, so that the skeletal mechanisms obtained under a single pressure condition or not applicable pressure range are excluded. Under relevant conditions as involved for comparisons for the detailed mechanism and preferred skeletal mechanism, the systematic comparisons on ignition delay times (IDTs), laminar flame speeds (LFSs), and species concentration profiles (SCPs) for different mechanisms are performed for ethylene combustion.
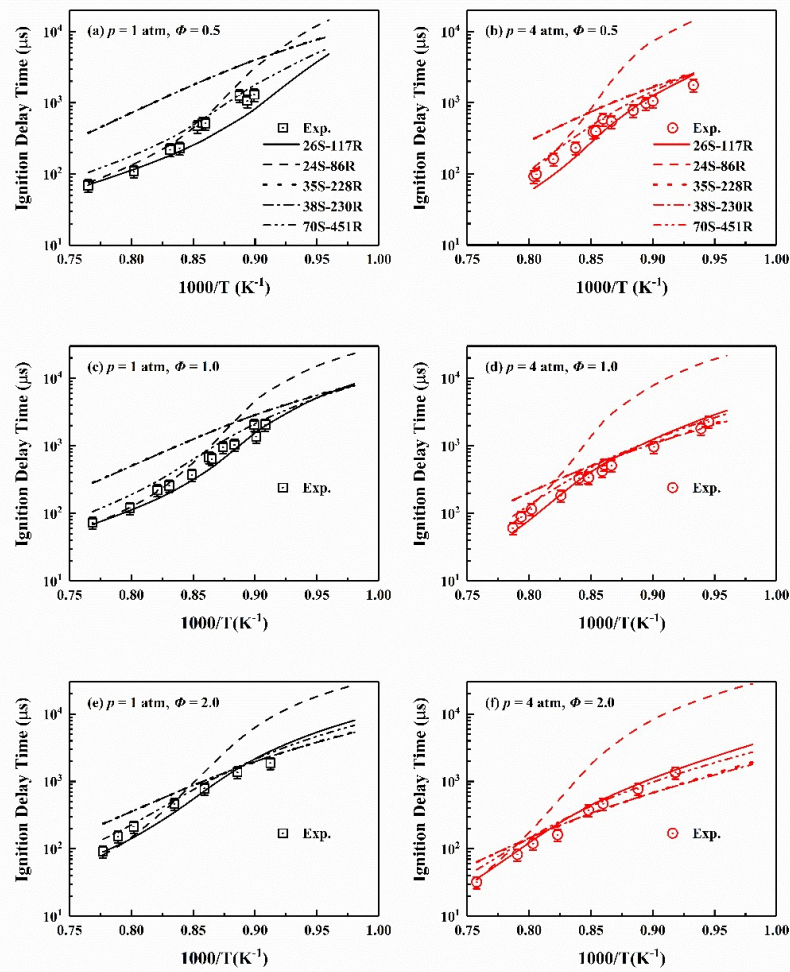

Fig. S2. IDTs for ethylene/air mixture predicted by different mechanisms under wide temperature range for p of 1, 4 atm and Φ of 0.5, 1.0, and 2.0.

Fig. S2 illustrates the comparisons of IDTs for ethylene/air mixture predicted by the five mechanisms under wide temperature range for p of 1, 4 atm and Φ of 0.5, 1.0, and 2.0. As can be noticed, the skeletal mechanism 24S-86R [11] always overestimates IDTs for corresponding conditions at temperatures lower than 1200 K. Whereas the skeletal mechanisms derived both

from USC-II [28], 35S-228R [49] and 38S-230R [63], present identical prediction results, and they overestimate the IDTs for corresponding conditions at temperatures higher than about 1200 K. Better predictions compared to the other mechanisms are provided by the skeletal mechanisms of 26S-117R and 70S-451R [44], the former coincides well with the corresponding experimental measurements.

Fig. S3 and Fig. S4 respectively provide the comparisons of LFSs for ethylene/air mixture predicted by different mechanisms under $T = 298$ K and p of 1, 2 atm and under T of 300 K, 373 K, and 443 K at $p = 1$ atm. The prediction results of LESs by different mechanisms don't present significant differences as those of IDTs. Considering these measured data are obtained from different experimental methods [34], the simulation results of these mechanisms can well reflect the variation of LESs with pressure and temperature for ethylene/air mixtures with different equivalence ratios.
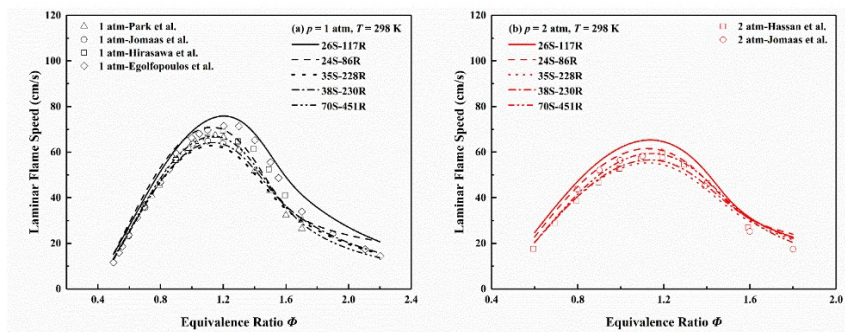

Fig. S3. LFSs for ethylene/air mixture predicted by different mechanisms under $T = 298$ K and p of 1, 2 atm.
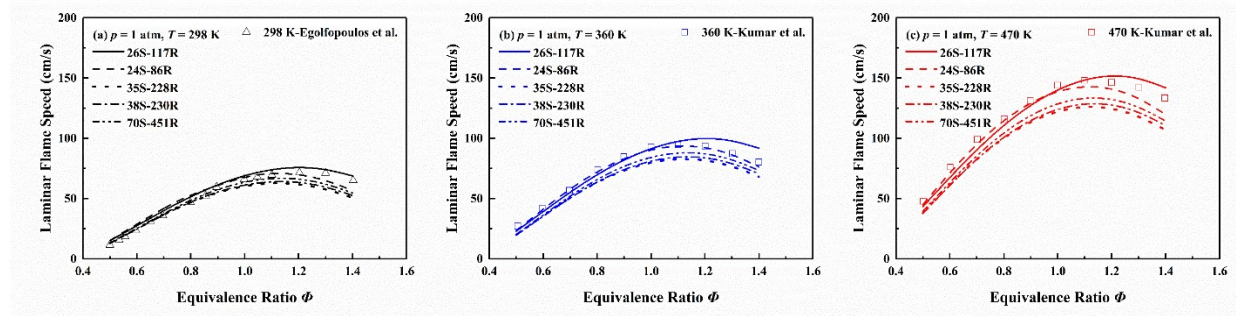

Fig. S4. LFSs for ethylene/air mixture predicted by different mechanisms under T of 300 K, 373 K, and 443 K at $p = 1$ atm.

Fig. S5 presents the comparisons of SCPs of fuel (C_2H_4) and major products (CO and CO_2) predicted by different mechanisms for $C_2H_4/O_2/N_2$ mixture under wide working conditions ($p = 1.0$ atm, $T = 773 - 900$ K, and $\Phi = 3$, 5, and 10). Compared to the indirect macroscopic prediction results of IDTs and LFSs, SCPs can more directly and accurately characterize the fuel oxidation process. One can observe that the skeletal mechanism 24S-86R [11] even fails to predict the occurrence of reactions in the investigated temperature range. Skeletal mechanisms of 35S-228R [49] and 38S-230R [63] yield basically identical predictions, but significantly deviate from the corresponding experimental data. The skeletal mechanisms of 26S-117R and 70S-451R [44] are qualified for revealing the evolution of fuel and major

combustion products with temperature during the oxidation of ethylene/air mixtures with different equivalence ratios. Meanwhile, the skeletal mechanism 26S-117R provide predictions that are in better agreement with corresponding experimental data.
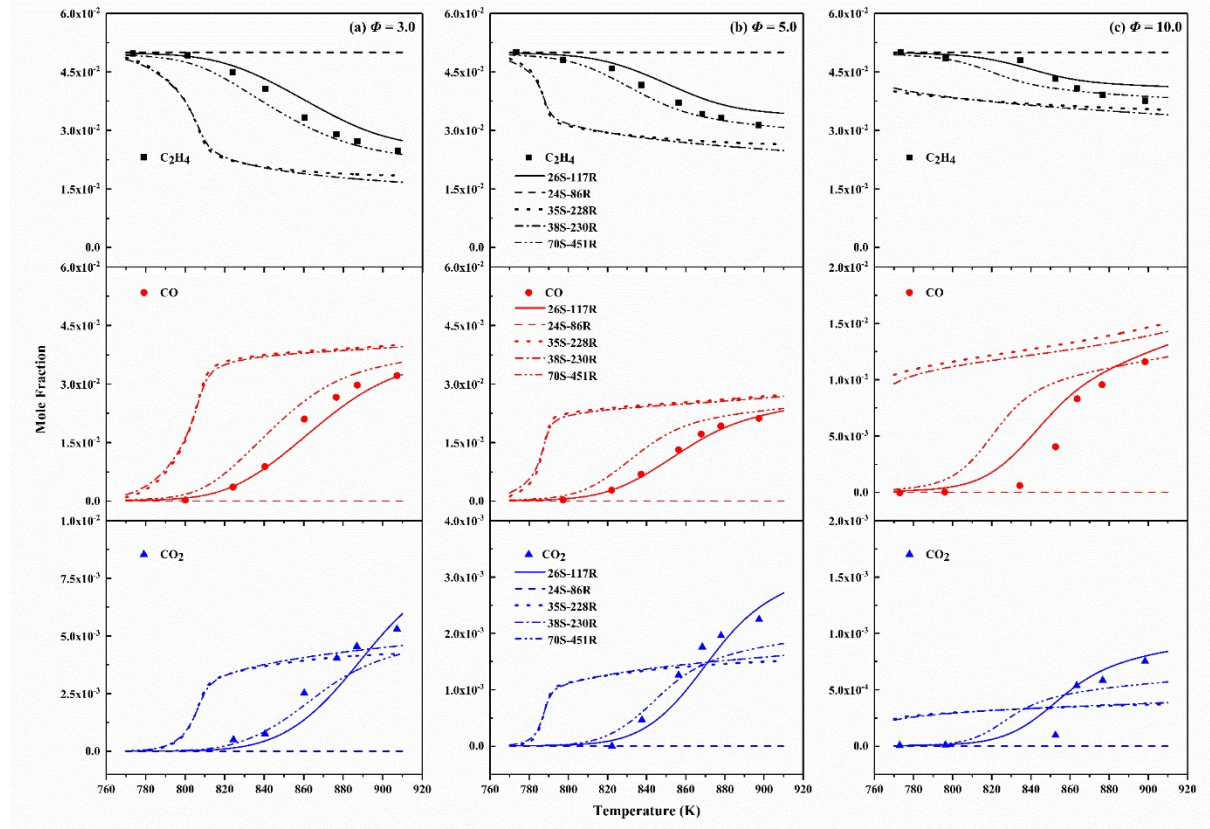

Fig. S5. SCPs of fuel and major products for $C_2H_4/O_2/N_2$ mixture predicted by different mechanisms under wide temperature range for Φ of 3.0, 5.0, and 10.0 at p = 1 atm.

Through detailed comparisons and discussions of the kinetic performances of the skeletal mechanism 26S-117R with those of other related skeletal mechanisms in Table 1, it is safely concluded that the mechanism has the advantage of favourable kinetic performance and compact size.

Reaction path analyses for ignition moments under relevant combustion conditions

Reaction path analyses around ignition moment of the ethylene/ vitiated air mixture are performed under initial temperature of 1000 K, pressure of 1, 4 atm, and equivalence ratios of 0.5, 1.0 and 2.0 to validate whether the skeletal mechanism retains key reaction paths. The normalized reaction fluxes of key reaction paths for the detailed mechanism and the skeletal mechanism 26S-117R are successively compared in Fig. S6 - Fig. S11. Though some of the normalized reaction flux values change to some extent after reduction due to the elimination of some species and reactions, as can be observed that the dominant key reaction paths are retained in the skeletal mechanism and it is qualified to characterize the reaction characteristics under the investigated working conditions.
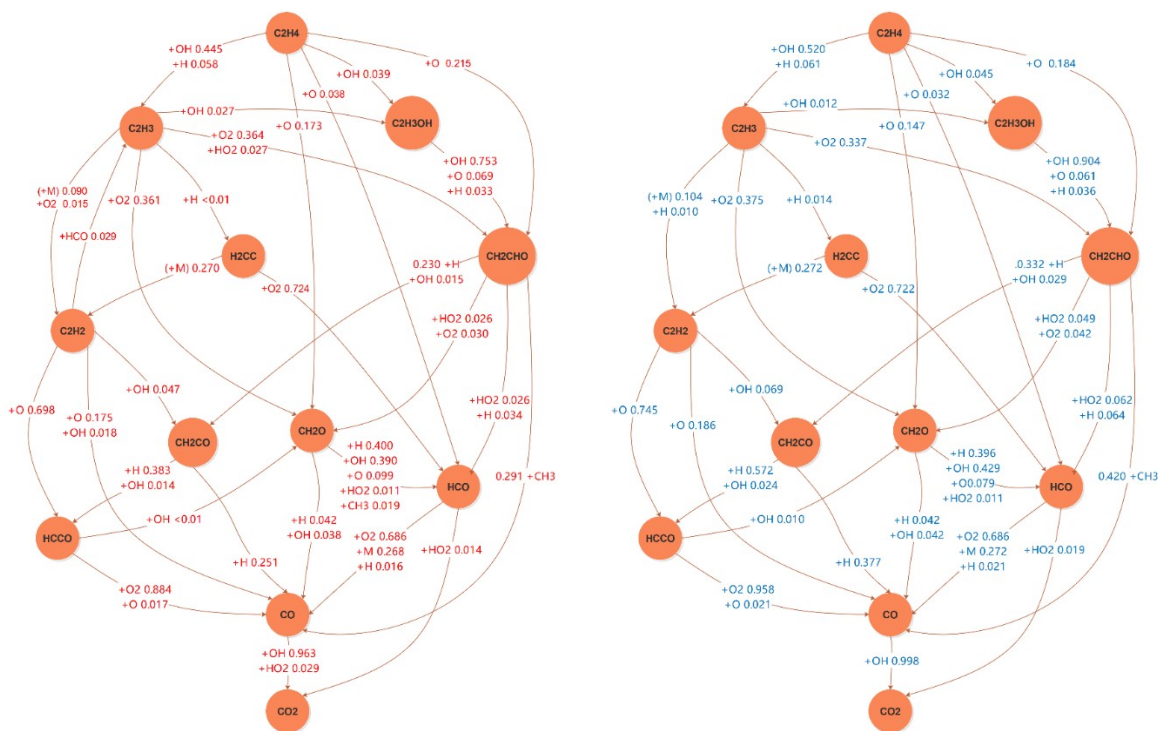
Fig. S6. Reaction path analysis of $T = 1000$ K, $p = 1.0$ atm, and $\Phi = 0.5$ for the detailed (left column) and skeletal (right column) mechanisms.
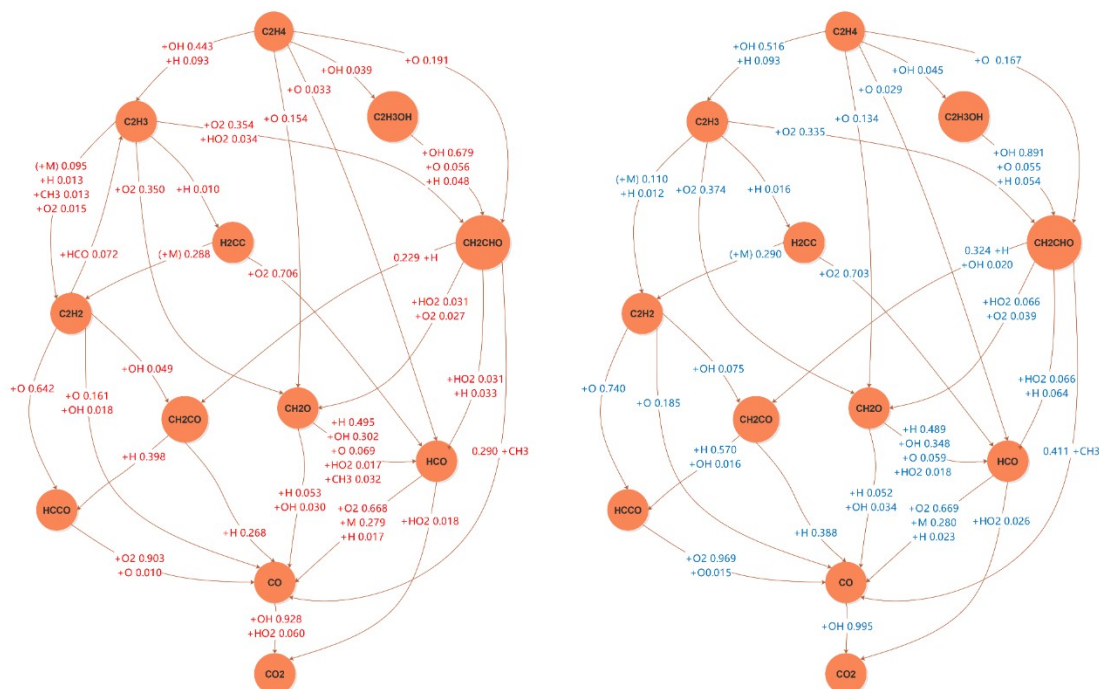

Fig. S7. Reaction path analysis of $T = 1000$ K, $p = 1.0$ atm, and $\Phi = 1.0$ for the detailed (left column) and skeletal (right column) mechanisms.
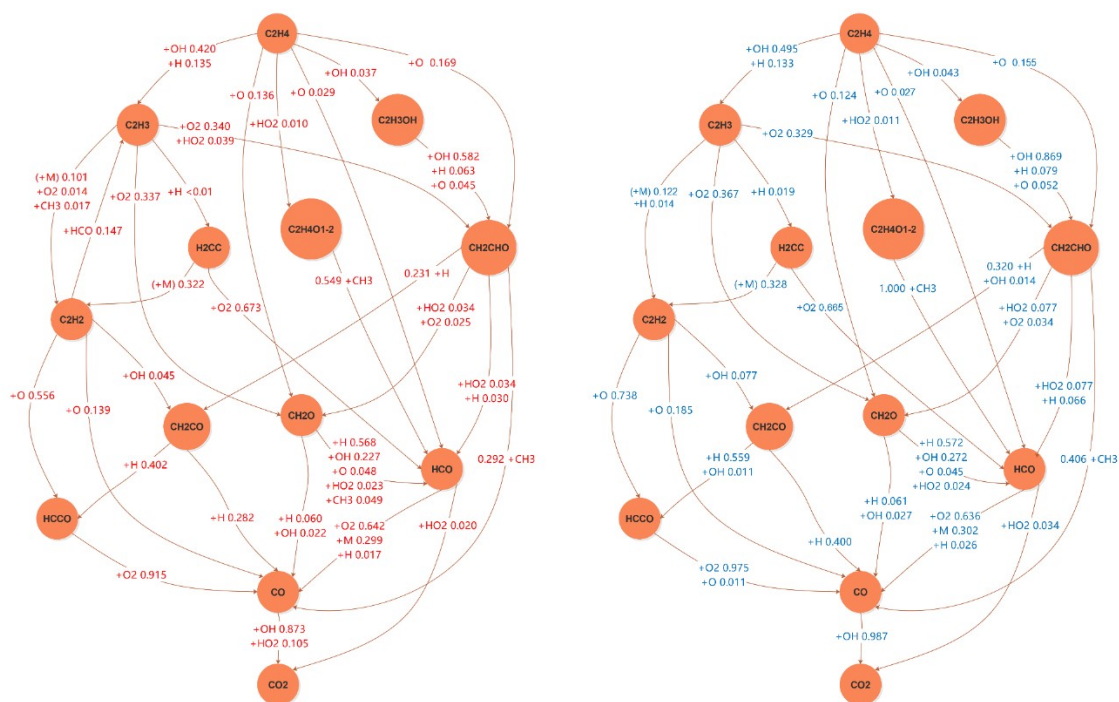
Fig. S8. Reaction path analysis of $T = 1000$ K, $p = 1.0$ atm, and $\Phi = 2.0$ for the detailed (left column) and skeletal (right column) mechanisms.
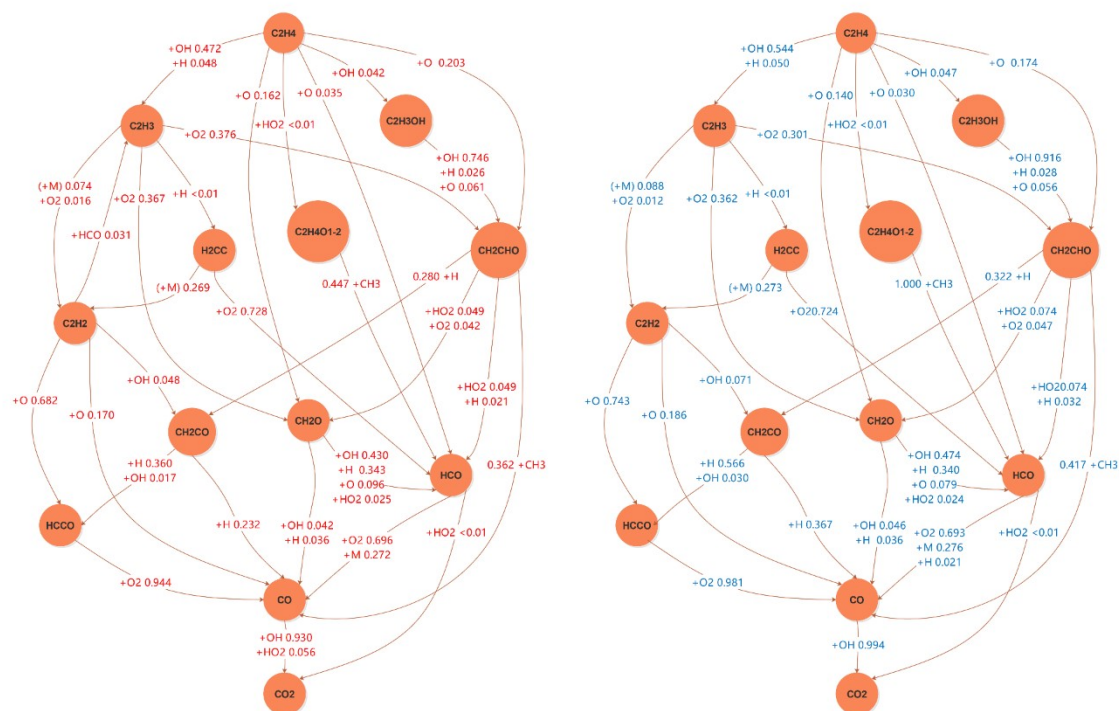

Fig. S9. Reaction path analysis of $T = 1000$ K, $p = 4.0$ atm, and $\Phi = 0.5$ for the detailed (left column) and skeletal (right column) mechanisms.

Fig. S10. Reaction path analysis of $T = 1000$ K, $p = 4.0$ atm, and $\Phi = 1.0$ for the detailed (left column) and skeletal (right column) mechanisms.
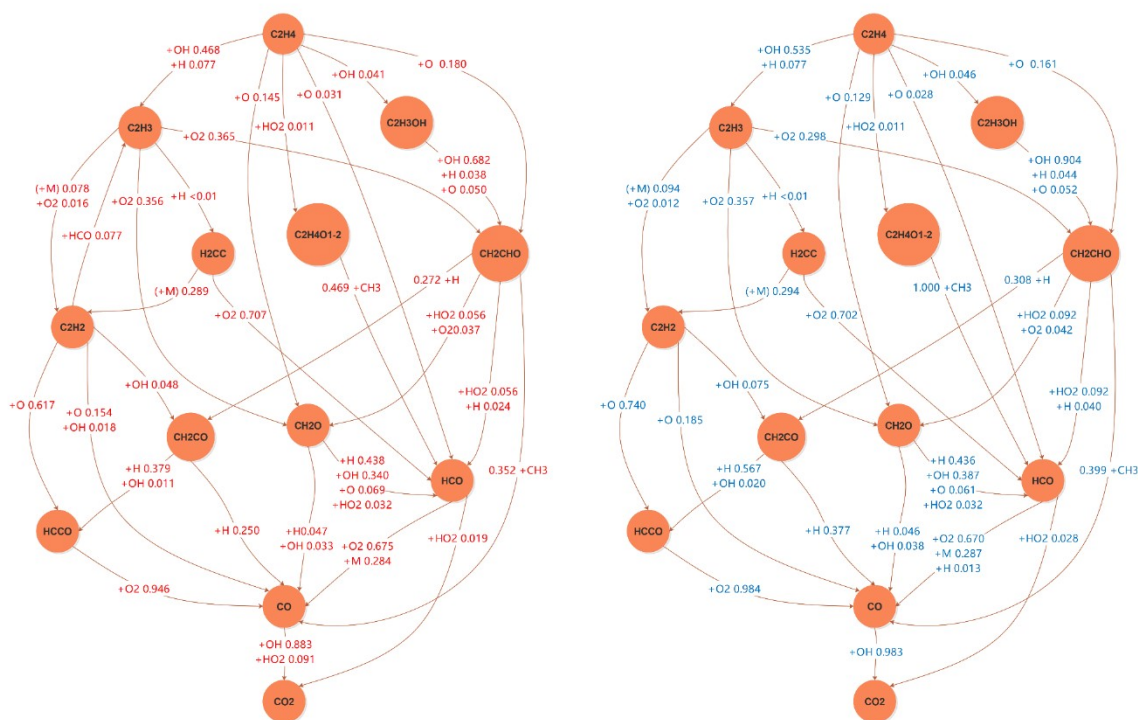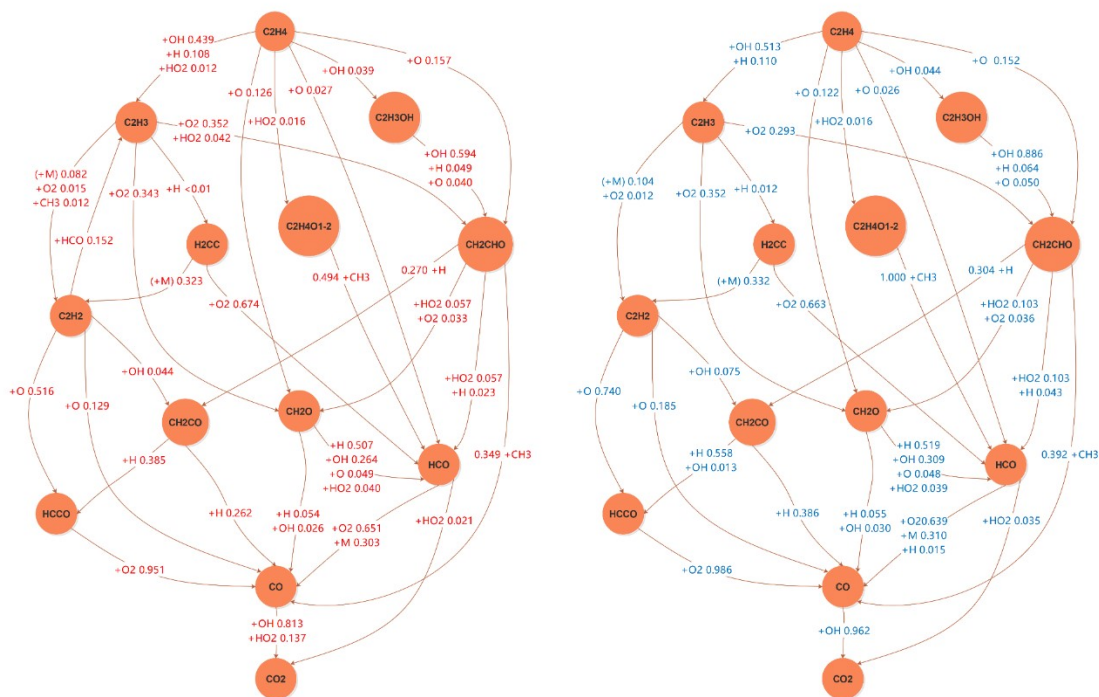

Fig. S11. Reaction path analysis of $T = 1000$ K, $p = 4.0$ atm, and $\Phi = 2.0$ for the detailed (left column) and skeletal (right column) mechanisms.

Comparisons on combustion simulation results with related works

Sun et al. [18] carried out combustion simulation studies for the scramjet mode ($\Phi = 0.26$) and the ramjet mode ($\Phi = 0.51$) of this combustor, the global mechanism of 6 species and 3 reactions (6S-3R) for ethylene-oxygen combustion proposed by Mawid et al. [14] was adopted in simulations. Besides, Gao et al. [17] conducted combustion simulation studies for the scramjet mode of the combustor, the global mechanism of 5 species and 2 reactions (5S-2R) for ethylene-oxygen combustion proposed by Westbrook et al. [15] was adopted in simulations. In the above studies, they provided simulation results for the pressure distribution profiles along the upper wall centerline and temperature contours of the central cross-section. Thus, the combustion simulation results of the ethylene skeletal mechanism 26S-117R are compared with available simulation results with these mechanisms.
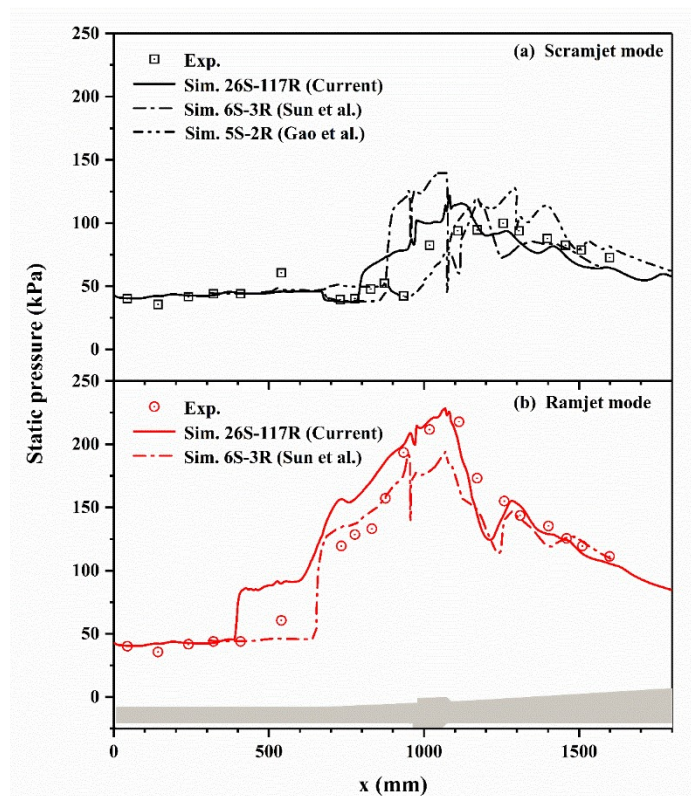

Fig. S12. Static pressure profiles along the upper wall centerline for the two combustion modes with different mechanisms.

Fig. S12 illustrates the comparisons of static pressure profiles along the upper wall centerline predicted by different mechanisms under the two modes. For the scramjet mode, there are large differences in the prediction results on pressure distribution of the combustor between different mechanisms. The simulation results of the global mechanism 6S-3R [14] used by Sun et al. [18] overestimate the pressure near the T1 cavity, while the simulation results of the global mechanism 5S-2R [15] used by Gao et al. [17] overestimate the pressure downstream of the T1 cavity. It is evident that the former predicts faster occurrence of reactions leading to a concentrated heat release from combustion around the T1 cavity, whereas the latter predicts slower occurrence of reactions causing combustion heat release to shift downstream of the

cavity. The simulation results of the skeletal mechanism 26S-117R provide better prediction of the occurrence of reactions, thereby it gives better predictions on the initial pressure rise location and the pressure rise ratio. For the ramjet mode, compared to the simulation results of the global mechanism 6S-3R [14], the skeletal mechanism 26S-117R better characterize the combustion intensity and distribution of heat release. The former underestimates the combustion intensity around the T1 cavity, resulting in unsatisfactory prediction results near here.
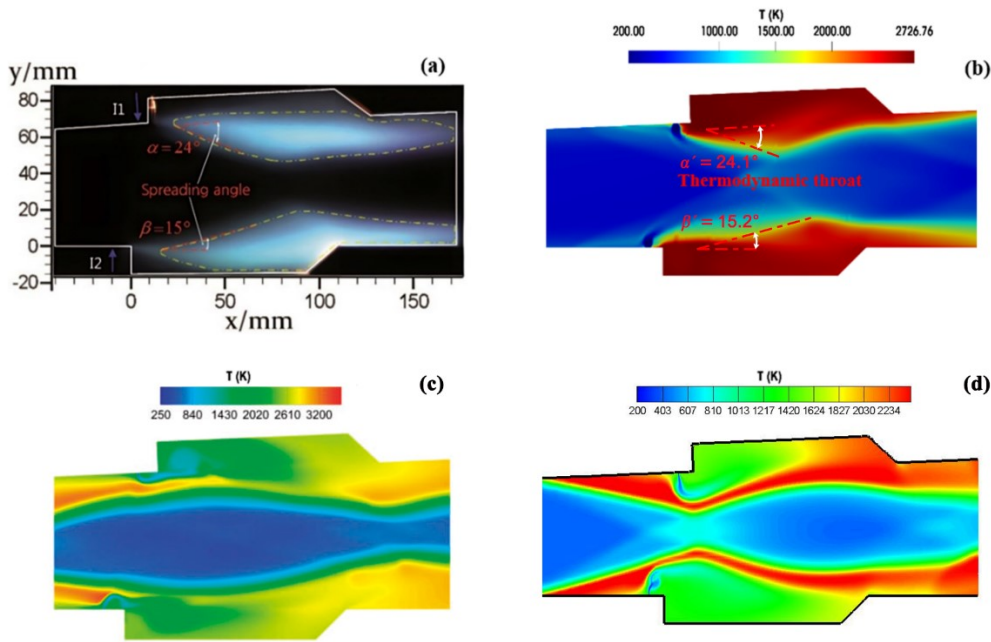

Fig. S13. Comparisons between the experimental flame luminosity image (a) and the numerical results for the scramjet mode. (b) numerical result of 26S-117R, (c) numerical result of 5S-2R, (d) numerical result of 6S-3R.
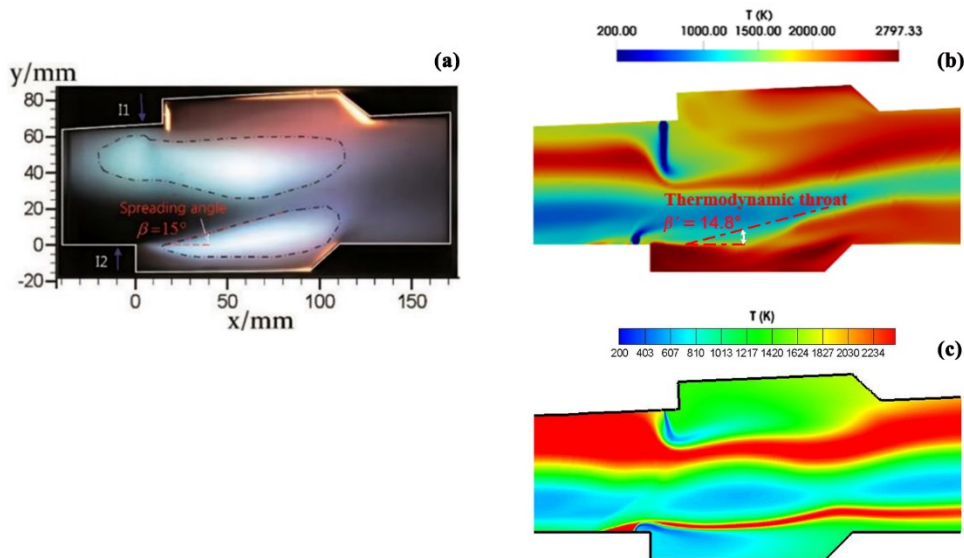

Fig. S14. Comparisons between the experimental flame luminosity image (a) and the numerical results for the ramjet mode. (b) numerical result of 26S-117R, (c) numerical result of 6S-3R.

Fig. S13 and Fig. S14 respectively present the comparisons of flame luminosity image in experiment and numerical results obtained by different mechanisms for the scramjet and ramjet modes. For the scramjet mode, the reaction zones simulated by 5S-2R [15] are mainly concentrated near the trailing edge of cavities, whereas the reaction intensity stimulated by 6S-3R [14] is so intensive that the thermodynamic throat formed by combustion is significantly shifted upstream of cavities. These features of their prediction results are consistent with the distribution characteristics of their pressure profiles observed in Figure S12. Compared to their simulation results, 26S-117R provides predictions that are in better agreement with experimental measurement of flame luminosity image. For the ramjet mode, 6S-3R [14] and 26S-117R provide good agreement in the prediction of flow characteristics. However, the former predicts lower reaction intensities in the two cavities, which is also proved in its pressure distribution profile in Figure 12. Therefore, it fails to reproduce the flame distribution characteristics within the cavities.

The detailed comparisons and discussions above further demonstrate the advantage of the skeletal mechanism 26S-117R obtained by the integrated reduction method in the combustion simulations for the ethylene-fueled scramjet combustor.